Hepatic JNK-mediated bile acid homeostasis regulates liver cancer through PPARα

Elisa Manieri[1,2,3], Laura Esteban-Lafuente[1], María Elena Rodríguez[1], Luis Leiva-Vega[1], Chaobo Chen[4], Francisco Javier Cubero[4], Tamera Barrett[5,6], Julie Cavanagh-Kyros[5,6], Davide Seruggia[7], Maria J. Monte[8], Jose J.G. Marin[8], Roger J. Davis[6,7], Alfonso Mora[1]*, Guadalupe Sabio[1]*.

[1]Centro Nacional de Investigaciones Cardiovasculares (CNIC), 28029 Madrid, Spain

[2]Centro Nacional de Biotecnología, CSIC, 28049, Madrid, Spain

[3]Current affiliation: Department of Medical Oncology and Center for Functional Cancer Epigenetics, Dana-Farber Cancer Institute, Harvard Medical School, Boston, MA 02215, USA

[4]Complutense University School of Medicine, 28040, Madrid, Spain

[5]Howard Hughes Medical Institute

[6]Program in Molecular Medicine, University of Massachusetts Medical School, Worcester, Massachusetts 01605, USA.

[7]Division of Hematology/Oncology, Boston Children's Hospital, Dana-Farber Cancer Institute, Harvard Medical School, Boston, MA, USA.

[8]Laboratory of Experimental Hepatology and Drug Targeting, National Institute for Study of Liver and Gastrointestinal Diseases (CIBERehd), 37007, University of Salamanca, Salamanca, Spain.

*To whom correspondence should be addressed

Running Title: JNK-PPARα in liver cancer development

Corresponding author:

Guadalupe Sabio

DVM, PhD.

Associate Professor

Centro Nacional de Investigaciones Cardiovasculares Carlos III

C/ Melchor Fernández Almagro, 3

28029 Madrid (Spain)

Phone (34) 91453 12 00 ext 2004

gsabio@cnic.es

Character count: 49189

ABSTRACT

cJun NH_2-terminal kinase (JNK) inhibition has been suggested as a potential treatment for insulin resistance and steatosis through activation of the transcription factor PPARα. However, the long-term consequences have not been evaluated. We found that hepatic JNK deficiency alters bile acid and cholesterol metabolism, resulting in hepatic expression of FGF15 and activation of ERK in cholangiocytes, which ultimately promotes their proliferation. Genetic inactivation of PPARα identifies PPARα hyperactivation as the molecular mechanism for these deleterious effects. Our analysis indicates that hepatic PPARα activation is oncogenic: PPARα deficiency protects mice against carcinogen-induced hepatocellular carcinoma under high fat diet (HFD) condition. These surprising results urge the re-consideration of using JNK inhibitors or PPAR agonists for the treatment of metabolic syndrome.

Keywords: Cell damage / cholangiocarcinoma / hepatocellular carcinoma / JNK / PPARalpha

INTRODUCTION

Liver cancer is the fifth most common cancer and the second leading cause of cancer deaths worldwide (El-Serag, Davila et al., 2003, Parkin, Bray et al., 2005). Metabolic syndrome is a newly recognized, but important risk factor thought to contribute to the increased incidence of hepatocellular carcinoma (HCC) (Klein, Dawson et al., 2014). Steatosis contributes to HCC development due to its association with oxidative stress and inflammation (Smedile & Bugianesi, 2005). Metabolic disorders are common among obese and diabetic patients, and hepatocellular injuries can occur due to increased fat accumulation in the liver. Non-alcoholic fatty liver disease (NAFLD) is extremely frequent in these patients (Caldwell, Crespo et al., 2004), and body weight excess is commonly associated with advanced disease (Neuschwander-Tetri, Brunt et al., 2003). Recent studies have led to the identification of hepatic cJun NH_2-terminal kinase (JNK) as a signal transduction pathway that is critically required for obesity-induced insulin resistance and steatosis (Manieri & Sabio, 2015). The cJun NH_2-terminal kinase (JNK) signaling pathway contributes to the development of obesity and insulin resistance (Sabio & Davis, 2010). Indeed, mice deficient for *Jnk* in hepatocytes are resistant to high fat diet (HFD)-induced insulin resistance and steatosis (Vernia, Cavanagh-Kyros et al., 2014); therefore, this signaling pathway represents a potential target for therapeutic intervention. Biochemical studies demonstrate that JNK suppresses PPARα activation in hepatocytes, affecting lipid metabolism and steatosis through the hepatokine FGF21 (encoded by a PPARα target gene) (Vernia, Cavanagh-Kyros et al., 2016, Vernia et al., 2014).

The transcription factor PPARα plays a pivotal role in intracellular free fatty acid (FFA) and triglyceride metabolism by regulating genes involved in fatty acid transport and degradation in mitochondria and peroxisomes (Evans, Barish et al., 2004, Gulick, Cresci et al., 1994, Unger & Zhou, 2001). PPARα is expressed primarily in liver, heart, and muscle

and is a major regulator of fatty acid transport, catabolism and energy homeostasis (Memon, Tecott et al., 2000). PPARα activation in the liver is increased in metabolic diseases and obesity (Memon et al., 2000), and PPARα agonists appear to be therapeutically beneficial in diabetes. In fact, PPARα protects against steatosis in the mouse (Ip, Farrell et al., 2003) and suppresses hepatic inflammation (Teoh, Williams et al., 2010). However, PPARα deficiency in mice increases susceptibility to diethylnitrosamine (DEN)-induced HCC (Zhang, Chu et al., 2014), but long-term studies in rodents showed an association of PPARα agonists with hepatic carcinogenesis (Holden & Tugwood, 1999). These findings conflict with the growth inhibitory effects reported for PPARα agonists in cancer cell lines, including HCC cell lines (Maggiora, Oraldi et al., 2010, Panigrahy, Kaipainen et al., 2008, Yamasaki, Kawabe et al., 2011). PPARα may therefore cause context-specific actions on liver cancer development.

The activation of PPARα modifies bile acid (BA) synthesis, conjugation and transport (Li & Chiang, 2009). Altered regulation of BA may protect against steatosis but could increase liver cancer development due to changes in FGF protein levels. Although FGF19 improves the glycemic response and reduces liver steatosis, it also induces liver cancer (Shapiro, Kolodziejczyk et al., 2018). These contrasting potential functions of BAs prompted us to examine whether lack of JNK in hepatocytes, and the resulting hyperactivation of PPARα, could alter BA homeostasis with subsequent deleterious effects. Elucidation of the contribution of JNK and PPARα to liver carcinogenesis may help the development of effective treatments against this malignancy.

RESULTS

Hepatic JNK-deficiency alters bile acid homeostasis

We have previously shown that hepatic JNK deficiency results in the activation of the nuclear transcription factor PPARα and protection against diet-induced insulin resistance and steatosis (Vernia et al., 2014). The activation of PPARα caused altered BA metabolism (Li & Chiang, 2009). We therefore examined BA in hepatic JNK deficient mice (L^{DKO}) and control mice (L^{WT}) at 6 months of age. We found that total BA concentration in the blood of L^{DKO} mice were significantly increased compared with L^{WT} mice (Fig 1A). The increase in circulating BA concentration is consistent with the possibility that L^{DKO} mice may suffer from cholestasis.

The analysis of bile collected from the gallbladder of L^{DKO} and L^{WT} mice revealed significantly increased amounts of BA relative to the amount of cholesterol and phosphatidylcholine (PC) (Fig 1B). Hepatic expression of genes related to hepatic PC synthesis (*Scd2*, *Chpt1*, and *Chkb*) or hepatocyte-mediated transport of PC (*Abcb4* and *Atp8b1*) and BA (*Abc11* and *Slc10a1*) was markedly increased in L^{DKO} mice (Supplementary Fig EV1A, B). Similarly, increased expression of genes related to cholesterol synthesis (*Hmgcs1, Hmgcr*) and BA synthesis (*Baat*, *Cyp8b1 and Cyp27a*) was detected in L^{DKO} mice (Fig 1C). These data are consistent with altered biosynthesis and secretion of both cholesterol and BA through PPARα activation.

Hepatic JNK-deficiency causes cholestasis and liver damage

It is established that cholangitis is a major risk factor for the development of cholangiocarcinoma (de Groen, Gores et al., 1999). We therefore examined the liver of mature adult L^{DKO} and L^{WT} mice. No evidence of hepatic disease was found in L^{WT} mice. Similarly, analysis of hepatic sections prepared from young adult L^{DKO} mice (age 4 months)

did not indicate the presence of liver pathology (Figure EV1C). However, at age 10 months, 82% of L^{DKO} mice displayed multifocal bile duct hyperplasia together with fibrosis and inflammatory cell infiltrates (Fig 1D). Cholangiocytes stained positively with PCNA, a marker for proliferation (Fig 1D). These changes were associated with increased expression of myeloid genes (*Cd68* and *Lyz*) and inflammatory cytokines (*Ifng*, *Tnf*, *Il10*, and *Il12a*) in the liver (Fig 1E), and increased liver damage, as suggested by the high levels of liver enzymes (ALT, AST, and γ-GT) in the blood of L^{DKO} mice (Fig 1F). The remaining L^{DKO} mice exhibited cholangiocarcinoma (6%) or appeared to be healthy (12%). At age 14 months, 95% of L^{DKO} mice displayed cholangiocarcinoma (Fig 2A) associated with fibrosis (Fig 2B) and a large increase in liver mass together with a significant increase in ALT and AST (Fig 2C). The remaining L^{DKO} mice (6%) exhibited cystic livers with bile duct hyperplasia. Histological analysis indicated increased staining of glutamine synthetase (GS) in liver tumor lesions, together with neoplastic nodules with positive staining of the ductular markers CK19 and Sox9 (Fig 2D). Together, these data confirm that the majority of mature mice with compound deficiency of JNK1 and JNK2 progressively develop cholangiocarcinoma.

The development of bile duct hyperplasia and cholangiocarcinoma in L^{DKO} mice was associated with increased hepatic expression of *Cytokeratin 19* (*Krt19*), a cholangiocyte-specific epithelial marker, the G protein-coupled BA receptor 1 (*Gpbar1*) and the apical sodium-dependent BA transporter (Asbt, gene symbol *Slc10a2*) both expressed in cholangiocytes (Keitel, Reinehr et al., 2007) (Dawson, Lan et al., 2009) (Figure 2E). The Notch receptor ligand *Jagged-1* promotes the formation of intrahepatic bile ducts (Piccoli & Spinner, 2001), and was overexpressed in the liver of L^{DKO} mice (Fig 2E). Moreover, Bone morphogenetic protein 4 (Bmp4) mediates cholestasis-induced fibrosis (Fan, Shen et al., 2006) and cooperates with FGF to promote the development of cholangiocytes from

hepatoblasts (Yanai, Tatsumi et al., 2008); expression of hepatic *Bmp4* was increased in L^{DKO} mice compared with L^{WT} mice (Fig 2E). Hepatoblasts maturate to cholangiocytes through activation of ERK pathway (Yang, Wang et al., 2017) and BA can increase proliferation by ERK activation through FXR/FGF15/FGR4 pathway (Li & Chiang, 2015). We evaluated this pathway in 6 months-old mice, before cancer has developed. In concordance with elevated BA production, we found high FXR activation as suggested by the high levels of its target genes (*Shp* and *Fgr4*) observed in L^{DKO} mice (Fig 2F). Moreover, while control mice did not expressed *Fgf15*, we could detect *Fgf15* in L^{DKO} livers (Fig 2F). In agreement with these results, histological analysis indicated increased staining of ERK phosphorylation in cholangiocytes from L^{DKO} mice compared with L^{WT} mice (Fig 2G). Together, these changes in FXR/FGF15/FGR4/ERK pathway may contribute to cholangiocyte maturation and proliferation from hepatoblast resulting in bile duct hyperplasia and development of cholangiocarcinoma detected in L^{DKO} mice.

PPARα deficiency reduces liver cancer in JNK1/2 deficient liver

To confirm that hyperactivation of PPARα is involved in the development of cholangiocarcinoma in L^{DKO} mice, we ablated the *Ppara* gene in L^{DKO} mice. In the resulting JNK1/2 plus PPARα liver-deficient-mice ($L^{PPARαDKO}$), both tumor burden and incidence were clearly reduced (Fig 3A) compared with L^{DKO} mice. The major changes in BA were also reversed (Fig 3B). This is consistent with reduced hepatic expression in $L^{PPARαDKO}$ mice of genes involved in cholesterol and BA synthesis (*Hmgcr*, *Baat*, *Cyp8b1 and Cyp27a*) and hepatocyte-mediated BA transport (*Abc11, Abc4, Abcg5, Abcg8)* (Fig 3C). Histological analyses indicated that PPARα deficiency increased liver steatosis, but reduced hallmarks of carcinogenesis (anisokaryosis, apoptosis, ductogenesis, dysplasia and mitosis) in $L^{PPARαDKO}$ compared with L^{DKO} mice (Fig 3D). Moreover, CK19 and SOX9

185 staining were increased in L^{DKO} mice compared with $L^{PPAR\alpha DKO}$ in agreement with
186 cholangiocyte proliferation. Furthermore, although liver tumor lesions in L^{DKO} mice became
187 prominently stained for glutamine synthetase (GS), reduced staining for glutamine
188 synthetase was observed in the liver of $L^{PPAR\alpha DKO}$ mice (Fig 3D). In addition, RT-qPCR
189 analysis indicated that both inflammation and cholangiocarcinoma markers were reduced
190 in $L^{PPAR\alpha DKO}$ mice compared with L^{DKO} mice (Fig 3E, F). This evidence suggests that
191 PPARα deficiency protected against the promotion of cholangiocyte proliferation in mice
192 lacking hepatocyte JNK1/2. To evaluate whether PPARα deficiency and subsequent
193 normalization of BA production blunted the FXR/FGF15/FGR4/ERK pathway, we
194 evaluated FXR target gene expression. Hepatic RT-qPCR analysis indicated that *Fgf15*,
195 *Shp* and *Fgr4* expression were reduced in $L^{PPAR\alpha DKO}$ mice compared with L^{DKO} mice (Fig
196 3G). This is consistent with the observation of lower levels of ERK activation, detected by
197 immunohistochemistry, in $L^{PPAR\alpha DKO}$ cholangiocytes (Fig 3H).
198
199 **PPARα deficiency protects against DEN-induced HCC development in HFD-fed mice**
200 Our analysis suggests that activation of PPARα may promote liver tumor development by
201 altering BA physiology. Increased BA induces the synthesis and secretion of inflammatory
202 cytokines in liver, which consequently results in liver injury (Miyake, Wang et al., 2000).
203 Recently, it has been shown that increased hepatic BA controls HCC development in HFD-
204 fed mice (Xie, Wang et al., 2016). To evaluate the role of PPARα in this context, we
205 administered DEN to WT and PPARαKO mice on postnatal day 14, and 6 weeks later
206 placed the animals on either a normal chow diet or a high-fat diet (HFD) in which 60% of
207 calories are fat-derived (Park, Lee et al., 2010). Livers were examined for signs of HCC 8
208 months after DEN injection (Fig 4A). On normal chow diet, the two genotypes showed no
209 significant differences in tumor number or size (Figu EV2). In contrast, on HFD, the mean

number of tumors per animal was lower in PPARαKO mice compared with WT counterparts (Fig 4B). Moreover, tumors were smaller in PPARαKO mice than in WT mice (Fig 4B). This protection against HCC development in HFD-fed PPARαKO mice explained the better survival (Fig 4C). RT-qPCR analysis of tumor and non-tumor tissues from WT and PPARαKO mice revealed reduced expression of the cell-cycle genes *Cdk2*, *Ccna1*, *Foxm1*, and *Cdc25c* in non-tumor samples from PPARαKO mice and enhanced expression of the cell-cycle regulatory genes *p21*, *Trp53*, *p19* and *p57* in PPARαKO tumor tissue (Fig 4D). Collectively, these data indicate that the absence of PPARα protects against DEN-induced HCC in HFD-fed mice.

PPARα deficiency protects from liver damage on HFD

DEN induces hepatocyte death associated with enhanced compensatory proliferation and augmented HCC development (Das, Garlick et al., 2011, Hui, Bakiri et al., 2007, Maeda, Kamata et al., 2005). DEN-induced apoptosis in liver tissue, measured by caspase 3 cleavage, was reduced in HFD-fed PPARαKO mice (Fig 4E). Moreover, analysis of ALT and AST levels induced by acute DEN treatment in HFD-fed mice revealed less liver damage in PPARαKO mice than in WT counterparts (Fig 4F). Additionally, ERK and STAT3, targets of FGF15/19 that modulate HCC development (Uriarte, Fernandez-Barrena et al., 2013, Uriarte, Latasa et al., 2015, Zhou, Luo et al., 2017), were less activated in livers of PPARαKO mice (Fig 4G).

However, there was no significant reduction in blood levels of the cytokines IL6, TNFα, IL1β, CCL2, and IFNγ in HFD-fed PPARαKO mice, suggesting that the lower acute DEN-induced liver damage was not associated with reduced inflammation (Fig EV3). After acute DEN injection, HFD-fed PPARαKO mice showed higher levels of the chemokines CXCL2 and CCL3 (Fig EV3), correlating with higher levels of markers of infiltration by immune

cells (Fig EV4). These results suggest that PPARα in the liver, and not in hematopoietic cells, promotes HCC development in HFD-fed WT animals.

To confirm the role of PPARα in hepatocytes, we tested HCC development in chimeras created by transplanting WT or PPARαKO bone marrow (BM) into lethally irradiated WT or PPARαKO recipients. Chronic-DEN-induced HCC development was strongly suppressed in reconstituted PPARαKO mice compared with reconstituted WT mice, irrespective of donor BM genotype. On HFD, reconstituted PPARαKO mice also developed significantly smaller tumors than their WT counterparts, again irrespective of donor BM genotype (Fig 4H). Despite the established role of PPARα as an immune-modulator (Daynes & Jones, 2002), our bone marrow transplantation experiments show that loss of PPARα in immune cells does not contribute to the protection observed in PPARαKO mice. Our analysis indicates that that the protection against HCC in HFD-fed PPARαKO mice is not primarily mediated by bone-marrow-derived cells.

DISCUSSION

The growing occurrence of liver cancer is due, in part, to an increasing prevalence of established risk factors, such as obesity and physical inactivity (Torre, Bray et al., 2015). HCC, in particular, is strongly associated with obesity and often appears after years of liver steatosis (Caldwell et al., 2004). In addition, long-term elevated BA levels are a risk factor for liver cancer development (Zhang, Zhou et al., 2015) and patients having elevated BA concentration and diabetes have a higher risk of developing HCC (Cui, Martin et al., 2018, Wu, Ge et al., 2010). Indeed, increased BA can lead to inflammation, apoptosis and necrosis of hepatocytes (Allen, Jaeschke et al., 2011, Jansen, Ghallab et al., 2017).

PPARα is an important modulator of liver metabolism controlling lipid and BA homeostasis, and its activation has been shown to decrease fatty liver disease (Abdelmegeed, Yoo et

al., 2011, Li & Chiang, 2009, Yeon, Choi et al., 2004). We report that JNK mediated repression of PPARα causes changes in BA homeostasis which suppress cholangiocyte proliferation. Consequently, JNK-deficiency stimulates cholangiocyte proliferation and promotes the development of cholangiocarcinoma. This increased proliferation is mediated by the altered BA metabolism and the elevated hepatic expression of FXR/FGF15/FGR4 that triggers ERK activation in cholangiocytes. Our results have strong translational implications for obesity treatment. Activation of FXR by BA triggers the secretion of FGF15/FGF19 in humans (Inagaki, Choi et al., 2005), and the beneficial effects of FGF family on the obese metabolic profile has been well characterized (Nies, Sancar et al., 2015). However, their clinical use has been debated due to their implication in promoting liver cancer formation by stimulating proliferation (Cui et al., 2018, Zhou et al., 2017). In fact, it has been recently suggested that this deleterious effect of FGF15/FGF19 is more evident under HFD conditions (Cui et al., 2018). Our results support this observation as we describe a tumorigenic effect of PPARα under HFD condition and predict a deleterious effect of using FGF analogs for the treatment of obese patients.

Hepatic PPARα is an important mediator of this regulatory cascade. In fact, PPARα deficiency dramatically suppresses the phenotypes induced by JNK deficiency. The role of PPARα in liver cancer is still unclear. While some studies have demonstrated that PPARα activation might promote liver cancer (Hays, Rusyn et al., 2005, Nishimura, Dewa et al., 2007, Peters, Cattley et al., 1997), others indicate that PPARα activation may be neutral or suppress liver cancer development (Cheung, Akiyama et al., 2004, Heindryckx, Colle et al., 2009, Morimura, Cheung et al., 2006, Takashima, Ito et al., 2008). This could be due to different experimental conditions used in these studies. It is established that the consumption of a HFD causes PPARα activation (Soltis, Kennedy et al., 2017). The HFD also causes enhanced BA production and secretion which leads to cell damage and

apoptosis, and the compensatory proliferation of surrounding cells (Sun, Beggs et al., 2016, Yoshitsugu, Kikuchi et al., 2019). Here we demonstrate that in WT mice PPARα promotes tumor development in a HFD DEN-induced model of liver cancer. These results contrast with the lack of effects of PPARα over tumor progression in WT mice fed with ND. The pro-tumorigenic effect of PPARα activation in WT mice is due, in part, to an alteration in BA metabolism that drives ERK activation. These conclusions are consistent with a recent report demonstrating that another nuclear receptor, PPARδ, is activated by HFD and promotes intestinal stem cells hyperproliferation driving to colon cancer (Beyaz, Mana et al., 2016). The data presented here identify obesity-induced PPARα activation as a critical factor in HCC development and progression. Moreover, our study provides evidence that in obesity the effect of PPARα is bone-marrow independent, and that a major inductor of liver cancer is the inhibition of the hepatic JNK.

Because of the role of JNK/PPARα/FGF signaling in lipid metabolism and carcinogenesis and their possible use for steatosis and obesity treatment, it is fundamental to understand the mechanism and conditions in which these signaling pathways might contribute to carcinogenic progression. JNK inhibition and PPARα activation are both potential therapeutic targets in obesity but our results urge to consider the risk of HCC development and other secondary effects during long-term treatments.

MATERIALS & METHODS

Animals

PPARα knock out mice (PPARαKO) (B6;129S4-Ppara^{tm1Gonz}/J; RRID:IMSR_JAX:008154) and Albumin cre mice (B6.Cg-Speer6-ps1$^{Tg(Alb-cre)21Mng}$/J; RRID:IMSR_JAX:003574) were purchased from the Jackson Laboratory and backcrossed for 10 generations to the C57BL/6J background (Jackson Laboratory; RRID:IMSR_JAX:000664). Mice with compound JNK1/2 deficiency in hepatocytes (L^{DKO}) have been described (Das et al., 2011, Das, Sabio et al., 2009). Genotypes were identified by PCR analysis of genomic DNA isolated from mouse tails. All experiments were performed in male mice. For tumor studies, PPARαKO mice at postnatal day 14 received a single i.p. injection of 50 mg/kg body weight diethylnitrosamine (DEN, Sigma-Aldrich, N0258) dissolved in saline. Six weeks after DEN treatment, mice were put on a high-fat diet (HFD, Research Diet Inc.) or standard chow diet *ad libitum* until sacrifice 8 months after DEN injection. One group of HFD-fed mice was used for Kaplan-Meier analysis. For acute response studies, 6-week-old PPARαKO mice and WT mice were fed the HFD for 13 weeks, given a single 100 mg/kg body weight i.p. injection of DEN, and sacrificed after 48 hours. Radiation chimeras were generated by exposing 2-month-old DEN-injected recipient mice to 2 x 650 Gy ionizing radiation and reconstituting with $2x10^7$ cells from donor bone marrow by tail vein injection. Two weeks after bone marrow transplant, mice were fed the HFD *ad libitum* until sacrifice 8 months after DEN injection. Before sacrifice, blood samples were taken for analysis of ALT/AST and cytokines. In all cases, mice were euthanized after overnight starvation. Mice were housed in a pathogen-free animal facility and kept on a 12-hour light/dark cycle at constant temperature and humidity. All animal experiments conformed to EU Directive 2010/63EU and Recommendation 2007/526/EC, enforced in Spanish law under Real Decreto 53/2013 and the Institutional Animal Care and Use Committee (IACUC) of the University of Massachusetts Medical School.

Serum analysis

Plasma activities of ALT and AST were assessed with the ALT and AST Reagent Kit (Biosystems Reagents) using a Benchmark Plus microplate spectrophotometer (Bio-Rad). Plasma concentration of non-sulfated bile acids were measured with the Bile Acid Assay Kit (Sigma-Aldrich) using a Fluoroskan Ascent fluorescence multiwell plate reader (Thermo Labsystems). Serum cytokine concentrations were measured by multiplexed ELISA (Millipore) with a Luminex 200 analyzer.

Biochemical analysis

Total liver proteins were extracted in lysis buffer (50 mM Tris-HCl pH 7.5, 1 mM EGTA, 1 mM EDTA pH 8.0, 50 mM NaF, 1 mM sodium glycerophosphate, 5 mM pyrophosphate, 0.27 M sucrose, 1% Triton X-100, 0.1 mM PMSF, 0.1% 2-mercaptoethanol, 1 mM sodium ortovanadate, 1 µg/ml leupeptin, 1 µg/ml aprotinin). Extracts were separated by SDS–PAGE and transferred to 0.2 µm pore size nitrocellulose membranes (Bio-Rad). Blots were probed with primary antibodies to caspase-3 (#9662), cleaved caspase-3 (#9661), phospho ERK (#9101; RRID:AB_330744), ERK (#9102), phospho STAT3 (#9145; RRID:AB_2491009), and Vinculin (V4505, Sigma; RRID:AB_477617). All antibodies were used at 1:1000 dilution. After washes, membranes were incubated with an appropriate horseradish peroxidase-conjugated secondary antibody (GE Healthcare), and signal was detected using an enhanced chemiluminescent substrate for the detection of horseradish peroxidase (Clarity Western ECL substrate; Bio-Rad).

Histochemistry

Histology was performed using tissue fixed in 10% formalin for 24h, dehydrated and embedded in paraffin. Sections (7 µm) were cut and stained using hematoxylin and eosin (American Master Tech Scientific). Sections were also incubated with Bouin´s fluid overnight, counter-stain with hematoxylin (Sigma), and then stained with Masson-

Trichrome stain (American Master Tech Scientific). Immunohistochemistry was performed by staining tissue sections with antibodies against PCNA (biotinylated from thermofisher MS-106-B; RRID:AB_64272), SOX9 (Abcam ab3697; RRID:AB_304012), glutamine synthetase (Abcam ab73593; RRID:AB_2247588), cytokeratin 19 (Abcam ab15463; RRID:AB_2281021) or phospho-p44/42 MAPK (Thr202/Tyr204) (Cell Signaling Technology #9101). Streptavidin- conjugated horseradish peroxidase (Biogenex), and the substrate 3,3'-diaminobenzidene (Vector Laboratories) were used followed by brief counter-staining with Mayer's hematoxylin (Sigma).

Analysis of biliary lipids

Bile was collected from the gall bladder following cholecystectomy. We determined cholesterol and phospholipids using an enzymatic assay (Wako). Total bile acids were measured using Hall's Bile Stain Kit (American MasterTech). Bile acid species were examined by a modification of the method described by (Ye, Liu et al., 2007) using an HPLC-MS/MS (6410 Triple Quad LC/MS, Agilent Technologies). Chromatographic separation was achieved with gradient elution using a Zorbax Eclipse XDB-C18 column (150 mm x 4.6 mm, 5 µm) kept at 35ºC and a flow rate of 500 µl/min. Initial mobile phase was 80:20 methanol/water, both containing 5 mM ammonium acetate and 0.01% formic acid, pH 4.6, and it was changed to 97:3 methanol/water over 9 min and then returned to 80:20 in 1 min. Electrospray ionization (ESI) in negative mode was used, with the following conditions: gas temperature 350ºC, gas flow 8 l/min, nebulizer 10 psi, capillary voltage 2500 V. MS/MS acquisition was performed in multiple reaction monitoring (MRM) mode using the specific *m/z* transitions: $[M-H]^-$ ion to 80,2 for taurine-conjugated bile acids and $[M-H]^-$ ion to 74 for glycine-conjugated bile acids. Free bile acids did not generate characteristic ion fragments, as reported by others (Ye et al., 2007), and transition from un-fragmented precursor molecular ions 407.1 to 407.1, 391.3 to 391.3 and 375.3 to 375.3 were selected for trihydroxylated, dihydroxylated and monohydroxylated free bile acids,

respectively.

Real time q-PCR

Total RNA was isolated from liver and tumor tissue using the RNeasy Mini Kit (Qiagen) with on-column DNase I-digestion. Complementary DNA was synthesized with the High-Capacity Complementary DNA Reverse Transcription Kit (Applied Biosystems). Taqman© assays were performed using the probes listed in Table 1 (Applied Biosystems). Sequences of primers used for quantitative real-time-polymerase chain reaction (qRT-PCR) are provided in Table 2. Expression levels were normalized to *Gapdh* and *Actb* mRNA. qRT-PCR was performed using the Fast SYBR Green system (Applied Biosystems) in a 7900HT Fast Real-time PCR thermal cycler (Applied Biosystems). A dissociation curve program was employed after each reaction to verify purity of the PCR products. The expression of mRNA was examined by quantitative PCR analysis using a 7500 Fast Real Time PCR machine.

QUANTIFICATION AND STATISTICAL ANALYSIS

Statistical analysis

Differences between groups were examined for statistical significance using 2-tailed unpaired Student's *t* test (with Welch's correction when variances were different) or ANOVA coupled to Bonferroni's post-test. Kaplan-Meier analysis was performed using the log-rank test. Statistical details and experimental n are specified in figure legends. Statistical analysis were performed with the GraphPad Prism 7 software (RRID:SCR_002798).

ACKNOWLEDGMENTS

We thank S. Bartlett for English editing and David Garlick (University of Massachusetts Medical School) for pathological examination of tissue sections. CNIC Advanced Imaging and Animal facility for technical support.

G.S. (RYC-2009-04972), F.J.C (RYC-2014-15242) are investigators of the Ramón y Cajal Program. E.M was awarded La Caixa fellowship. This work was funded by grants supported in part by funds from European Regional Development Fund (ERDF): to G.S. European Union's Seventh Framework Programme (FP7/2007-2013) ERC 260464, EFSD/Lilly European Diabetes Research Programme Dr Sabio, 2017 Leonardo Grant for Researchers and Cultural Creators, BBVA Foundation (Investigadores-BBVA-2017) IN[17]_BBM_BAS_0066, MINECO-FEDER SAF2016-79126-R, and Comunidad de Madrid IMMUNOTHERCAN-CM S2010/BMD-2326 and B2017/BMD-3733; F.J.C. EXOHEP-CM S2017/BMD-3727 and the COST Action CA17112.; F.J.C. MINECO Retos SAF2016-78711, the AMMF Cholangiocarcinoma Charity 2018/117, NanoLiver-CM Y2018/NMT-4949, UCM-25-2019, ERAB EA/18-14,. F.J.C. is a Gilead Liver Research Scholar. R.J.D: Grant DK R01 DK107220 from the National Institutes of Health; and to JJGM: PI16/00598 from Carlos III Institute of Health, Spain. The CNIC is supported by the Ministerio de Ciencia, Innovación y Universidades (MCNU) and the Pro CNIC Foundation, and is a Severo Ochoa Center of Excellence (SEV-2015-0505).

Author Contributions

G.S. and A.M. conceived and supervised this project, E.M. and A.M. performed the experiments and prepared figures, G.S, A.M., R.J.D. and E.M. designed, developed the hypothesis, G.S, R.J. D, E.M, A.M., M J. M, J J.G. M analyzed and interpreted the data. L. E-L., T-L, M. E. R, D. S, C.C., F. J. C., L. L-V, T.B, J. C-K participated in the experiments. E.M., A.M and G.S. wrote the manuscript with input from all authors.

Conflict of Interest

The authors declare no potential conflict of interest.

REFERENCES

Abdelmegeed MA, Yoo SH, Henderson LE, Gonzalez FJ, Woodcroft KJ, Song BJ (2011) PPARalpha expression protects male mice from high fat-induced nonalcoholic fatty liver. *The Journal of nutrition* 141: 603-10

Allen K, Jaeschke H, Copple BL (2011) Bile acids induce inflammatory genes in hepatocytes: a novel mechanism of inflammation during obstructive cholestasis. *The American journal of pathology* 178: 175-86

Beyaz S, Mana MD, Roper J, Kedrin D, Saadatpour A, Hong SJ, Bauer-Rowe KE, Xifaras ME, Akkad A, Arias E, Pinello L, Katz Y, Shinagare S, Abu-Remaileh M, Mihaylova MM, Lamming DW, Dogum R, Guo G, Bell GW, Selig M et al. (2016) High-fat diet enhances stemness and tumorigenicity of intestinal progenitors. *Nature* 531: 53-8

Caldwell SH, Crespo DM, Kang HS, Al-Osaimi AM (2004) Obesity and hepatocellular carcinoma. *Gastroenterology* 127: S97-103

Cheung C, Akiyama TE, Ward JM, Nicol CJ, Feigenbaum L, Vinson C, Gonzalez FJ (2004) Diminished hepatocellular proliferation in mice humanized for the nuclear receptor peroxisome proliferator-activated receptor alpha. *Cancer research* 64: 3849-54

Cui G, Martin RC, Jin H, Liu X, Pandit H, Zhao H, Cai L, Zhang P, Li W, Li Y (2018) Up-regulation of FGF15/19 signaling promotes hepatocellular carcinoma in the background of fatty liver. *J Exp Clin Cancer Res* 37: 136

Das M, Garlick DS, Greiner DL, Davis RJ (2011) The role of JNK in the development of hepatocellular carcinoma. *Genes & development* 25: 634-45

Das M, Sabio G, Jiang F, Rincon M, Flavell RA, Davis RJ (2009) Induction of hepatitis by JNK-mediated expression of TNF-alpha. *Cell* 136: 249-60

Dawson PA, Lan T, Rao A (2009) Bile acid transporters. *J Lipid Res* 50: 2340-57

Daynes RA, Jones DC (2002) Emerging roles of PPARs in inflammation and immunity. *Nature reviews Immunology* 2: 748-59

de Groen PC, Gores GJ, LaRusso NF, Gunderson LL, Nagorney DM (1999) Biliary tract cancers. *N Engl J Med* 341: 1368-78

El-Serag HB, Davila JA, Petersen NJ, McGlynn KA (2003) The continuing increase in the incidence of hepatocellular carcinoma in the United States: an update. *Annals of internal medicine* 139: 817-23

Evans RM, Barish GD, Wang YX (2004) PPARs and the complex journey to obesity. *Nature medicine* 10: 355-61

Fan J, Shen H, Sun Y, Li P, Burczynski F, Namaka M, Gong Y (2006) Bone morphogenetic protein 4 mediates bile duct ligation induced liver fibrosis through activation of Smad1 and ERK1/2 in rat hepatic stellate cells. *J Cell Physiol* 207: 499-505

Gulick T, Cresci S, Caira T, Moore DD, Kelly DP (1994) The peroxisome proliferator-activated receptor regulates mitochondrial fatty acid oxidative enzyme gene expression. *Proceedings of the National Academy of Sciences of the United States of America* 91: 11012-6

Hays T, Rusyn I, Burns AM, Kennett MJ, Ward JM, Gonzalez FJ, Peters JM (2005) Role of peroxisome proliferator-activated receptor-alpha (PPARalpha) in bezafibrate-induced hepatocarcinogenesis and cholestasis. *Carcinogenesis* 26: 219-27

Heindryckx F, Colle I, Van Vlierberghe H (2009) Experimental mouse models for hepatocellular carcinoma research. *International journal of experimental pathology* 90: 367-86

Holden PR, Tugwood JD (1999) Peroxisome proliferator-activated receptor alpha: role in rodent liver cancer and species differences. *Journal of molecular endocrinology* 22: 1-8

Hui L, Bakiri L, Mairhorfer A, Schweifer N, Haslinger C, Kenner L, Komnenovic V, Scheuch H, Beug H, Wagner EF (2007) p38alpha suppresses normal and cancer cell proliferation by antagonizing the JNK-c-Jun pathway. *Nature genetics* 39: 741-9

Inagaki T, Choi M, Moschetta A, Peng L, Cummins CL, McDonald JG, Luo G, Jones SA, Goodwin B, Richardson JA, Gerard RD, Repa JJ, Mangelsdorf DJ, Kliewer SA (2005) Fibroblast growth factor 15 functions as an enterohepatic signal to regulate bile acid homeostasis. *Cell metabolism* 2: 217-25

Ip E, Farrell GC, Robertson G, Hall P, Kirsch R, Leclercq I (2003) Central role of PPARalpha-dependent hepatic lipid turnover in dietary steatohepatitis in mice. *Hepatology* 38: 123-32

Jansen PL, Ghallab A, Vartak N, Reif R, Schaap FG, Hampe J, Hengstler JG (2017) The ascending pathophysiology of cholestatic liver disease. *Hepatology* 65: 722-738

Keitel V, Reinehr R, Gatsios P, Rupprecht C, Gorg B, Selbach O, Haussinger D, Kubitz R (2007) The G-protein coupled bile salt receptor TGR5 is expressed in liver sinusoidal endothelial cells. *Hepatology* 45: 695-704

Klein J, Dawson LA, Tran TH, Adeyi O, Purdie T, Sherman M, Brade A (2014) Metabolic syndrome-related hepatocellular carcinoma treated by volumetric modulated arc therapy. *Current oncology* 21: e340-4

Li T, Chiang JY (2009) Regulation of bile acid and cholesterol metabolism by PPARs. *PPAR research* 2009: 501739

Li T, Chiang JY (2015) Bile acids as metabolic regulators. *Curr Opin Gastroenterol* 31: 159-65

Maeda S, Kamata H, Luo JL, Leffert H, Karin M (2005) IKKbeta couples hepatocyte death to cytokine-driven compensatory proliferation that promotes chemical hepatocarcinogenesis. *Cell* 121: 977-90

Maggiora M, Oraldi M, Muzio G, Canuto RA (2010) Involvement of PPARalpha and PPARgamma in apoptosis and proliferation of human hepatocarcinoma HepG2 cells. *Cell biochemistry and function* 28: 571-7

Manieri E, Sabio G (2015) Stress kinases in the modulation of metabolism and energy balance. *Journal of molecular endocrinology* 55: R11-22

Memon RA, Tecott LH, Nonogaki K, Beigneux A, Moser AH, Grunfeld C, Feingold KR (2000) Up-regulation of peroxisome proliferator-activated receptors (PPAR-alpha) and PPAR-gamma messenger ribonucleic acid expression in the liver in murine obesity: troglitazone induces expression of PPAR-gamma-responsive adipose tissue-specific genes in the liver of obese diabetic mice. *Endocrinology* 141: 4021-31

Miyake JH, Wang SL, Davis RA (2000) Bile acid induction of cytokine expression by macrophages correlates with repression of hepatic cholesterol 7alpha-hydroxylase. *The Journal of biological chemistry* 275: 21805-8

523 Morimura K, Cheung C, Ward JM, Reddy JK, Gonzalez FJ (2006) Differential
524 susceptibility of mice humanized for peroxisome proliferator-activated receptor alpha
525 to Wy-14,643-induced liver tumorigenesis. *Carcinogenesis* 27: 1074-80
526 Neuschwander-Tetri BA, Brunt EM, Wehmeier KR, Oliver D, Bacon BR (2003)
527 Improved nonalcoholic steatohepatitis after 48 weeks of treatment with the PPAR-
528 gamma ligand rosiglitazone. *Hepatology* 38: 1008-17
529 Nies VJ, Sancar G, Liu W, van Zutphen T, Struik D, Yu RT, Atkins AR, Evans RM, Jonker
530 JW, Downes MR (2015) Fibroblast Growth Factor Signaling in Metabolic Regulation.
531 *Front Endocrinol (Lausanne)* 6: 193
532 Nishimura J, Dewa Y, Muguruma M, Kuroiwa Y, Yasuno H, Shima T, Jin M, Takahashi M,
533 Umemura T, Mitsumori K (2007) Effect of fenofibrate on oxidative DNA damage and
534 on gene expression related to cell proliferation and apoptosis in rats. *Toxicological*
535 *sciences : an official journal of the Society of Toxicology* 97: 44-54
536 Panigrahy D, Kaipainen A, Huang S, Butterfield CE, Barnes CM, Fannon M, Laforme AM,
537 Chaponis DM, Folkman J, Kieran MW (2008) PPARalpha agonist fenofibrate
538 suppresses tumor growth through direct and indirect angiogenesis inhibition.
539 *Proceedings of the National Academy of Sciences of the United States of America* 105:
540 985-90
541 Park EJ, Lee JH, Yu GY, He G, Ali SR, Holzer RG, Osterreicher CH, Takahashi H, Karin M
542 (2010) Dietary and genetic obesity promote liver inflammation and tumorigenesis by
543 enhancing IL-6 and TNF expression. *Cell* 140: 197-208
544 Parkin DM, Bray F, Ferlay J, Pisani P (2005) Global cancer statistics, 2002. *CA: a cancer*
545 *journal for clinicians* 55: 74-108
546 Peters JM, Cattley RC, Gonzalez FJ (1997) Role of PPAR alpha in the mechanism of
547 action of the nongenotoxic carcinogen and peroxisome proliferator Wy-14,643.
548 *Carcinogenesis* 18: 2029-33
549 Piccoli DA, Spinner NB (2001) Alagille syndrome and the Jagged1 gene. *Semin Liver*
550 *Dis* 21: 525-34
551 Sabio G, Davis RJ (2010) cJun NH2-terminal kinase 1 (JNK1): roles in metabolic
552 regulation of insulin resistance. *Trends Biochem Sci* 35: 490-6
553 Shapiro H, Kolodziejczyk AA, Halstuch D, Elinav E (2018) Bile acids in glucose
554 metabolism in health and disease. *The Journal of experimental medicine* 215: 383-396
555 Smedile A, Bugianesi E (2005) Steatosis and hepatocellular carcinoma risk. *European*
556 *review for medical and pharmacological sciences* 9: 291-3
557 Soltis AR, Kennedy NJ, Xin X, Zhou F, Ficarro SB, Yap YS, Matthews BJ, Lauffenburger
558 DA, White FM, Marto JA, Davis RJ, Fraenkel E (2017) Hepatic Dysfunction Caused by
559 Consumption of a High-Fat Diet. *Cell reports* 21: 3317-3328
560 Sun L, Beggs K, Borude P, Edwards G, Bhushan B, Walesky C, Roy N, Manley MW, Jr.,
561 Gunewardena S, O'Neil M, Li H, Apte U (2016) Bile acids promote diethylnitrosamine-
562 induced hepatocellular carcinoma via increased inflammatory signaling. *American*
563 *journal of physiology Gastrointestinal and liver physiology* 311: G91-G104
564 Takashima K, Ito Y, Gonzalez FJ, Nakajima T (2008) Different mechanisms of DEHP-
565 induced hepatocellular adenoma tumorigenesis in wild-type and Ppar alpha-null mice.
566 *Journal of occupational health* 50: 169-80
567 Teoh NC, Williams J, Hartley J, Yu J, McCuskey RS, Farrell GC (2010) Short-term
568 therapy with peroxisome proliferation-activator receptor-alpha agonist Wy-14,643

569 protects murine fatty liver against ischemia-reperfusion injury. *Hepatology* 51: 996-
570 1006
571 Torre LA, Bray F, Siegel RL, Ferlay J, Lortet-Tieulent J, Jemal A (2015) Global cancer
572 statistics, 2012. *CA: a cancer journal for clinicians* 65: 87-108
573 Unger RH, Zhou YT (2001) Lipotoxicity of beta-cells in obesity and in other causes of
574 fatty acid spillover. *Diabetes* 50 Suppl 1: S118-21
575 Uriarte I, Fernandez-Barrena MG, Monte MJ, Latasa MU, Chang HC, Carotti S,
576 Vespasiani-Gentilucci U, Morini S, Vicente E, Concepcion AR, Medina JF, Marin JJ,
577 Berasain C, Prieto J, Avila MA (2013) Identification of fibroblast growth factor 15 as a
578 novel mediator of liver regeneration and its application in the prevention of post-
579 resection liver failure in mice. *Gut* 62: 899-910
580 Uriarte I, Latasa MU, Carotti S, Fernandez-Barrena MG, Garcia-Irigoyen O, Elizalde M,
581 Urtasun R, Vespasiani-Gentilucci U, Morini S, de Mingo A, Mari M, Corrales FJ, Prieto J,
582 Berasain C, Avila MA (2015) Ileal FGF15 contributes to fibrosis-associated
583 hepatocellular carcinoma development. *Int J Cancer* 136: 2469-75
584 Vernia S, Cavanagh-Kyros J, Barrett T, Tournier C, Davis RJ (2016) Fibroblast Growth
585 Factor 21 Mediates Glycemic Regulation by Hepatic JNK. *Cell reports* 14: 2273-80
586 Vernia S, Cavanagh-Kyros J, Garcia-Haro L, Sabio G, Barrett T, Jung DY, Kim JK, Xu J,
587 Shulha HP, Garber M, Gao G, Davis RJ (2014) The PPARalpha-FGF21 Hormone Axis
588 Contributes to Metabolic Regulation by the Hepatic JNK Signaling Pathway. *Cell*
589 *metabolism* 20: 512-25
590 Wu X, Ge H, Lemon B, Vonderfecht S, Weiszmann J, Hecht R, Gupte J, Hager T, Wang Z,
591 Lindberg R, Li Y (2010) FGF19-induced hepatocyte proliferation is mediated through
592 FGFR4 activation. *The Journal of biological chemistry* 285: 5165-70
593 Xie G, Wang X, Huang F, Zhao A, Chen W, Yan J, Zhang Y, Lei S, Ge K, Zheng X, Liu J, Su
594 M, Liu P, Jia W (2016) Dysregulated hepatic bile acids collaboratively promote liver
595 carcinogenesis. *Int J Cancer* 139: 1764-75
596 Yamasaki D, Kawabe N, Nakamura H, Tachibana K, Ishimoto K, Tanaka T, Aburatani H,
597 Sakai J, Hamakubo T, Kodama T, Doi T (2011) Fenofibrate suppresses growth of the
598 human hepatocellular carcinoma cell via PPARalpha-independent mechanisms.
599 *European journal of cell biology* 90: 657-64
600 Yanai M, Tatsumi N, Hasunuma N, Katsu K, Endo F, Yokouchi Y (2008) FGF signaling
601 segregates biliary cell-lineage from chick hepatoblasts cooperatively with BMP4 and
602 ECM components in vitro. *Dev Dyn* 237: 1268-83
603 Yang L, Wang WH, Qiu WL, Guo Z, Bi E, Xu CR (2017) A single-cell transcriptomic
604 analysis reveals precise pathways and regulatory mechanisms underlying hepatoblast
605 differentiation. *Hepatology* 66: 1387-1401
606 Ye L, Liu S, Wang M, Shao Y, Ding M (2007) High-performance liquid chromatography-
607 tandem mass spectrometry for the analysis of bile acid profiles in serum of women
608 with intrahepatic cholestasis of pregnancy. *J Chromatogr B Analyt Technol Biomed Life*
609 *Sci* 860: 10-7
610 Yeon JE, Choi KM, Baik SH, Kim KO, Lim HJ, Park KH, Kim JY, Park JJ, Kim JS, Bak YT,
611 Byun KS, Lee CH (2004) Reduced expression of peroxisome proliferator-activated
612 receptor-alpha may have an important role in the development of non-alcoholic fatty
613 liver disease. *Journal of gastroenterology and hepatology* 19: 799-804

614 Yoshitsugu R, Kikuchi K, Iwaya H, Fujii N, Hori S, Lee DG, Ishizuka S (2019) Alteration
615 of Bile Acid Metabolism by a High-Fat Diet Is Associated with Plasma Transaminase
616 Activities and Glucose Intolerance in Rats. *Journal of nutritional science and*
617 *vitaminology* 65: 45-51
618 Zhang N, Chu ES, Zhang J, Li X, Liang Q, Chen J, Chen M, Teoh N, Farrell G, Sung JJ, Yu J
619 (2014) Peroxisome proliferator activated receptor alpha inhibits
620 hepatocarcinogenesis through mediating NF-kappaB signaling pathway. *Oncotarget* 5:
621 8330-40
622 Zhang W, Zhou L, Yin P, Wang J, Lu X, Wang X, Chen J, Lin X, Xu G (2015) A weighted
623 relative difference accumulation algorithm for dynamic metabolomics data: long-term
624 elevated bile acids are risk factors for hepatocellular carcinoma. *Scientific reports* 5:
625 8984
626 Zhou M, Luo J, Chen M, Yang H, Learned RM, DePaoli AM, Tian H, Ling L (2017) Mouse
627 species-specific control of hepatocarcinogenesis and metabolism by FGF19/FGF15.
628 *Journal of hepatology* 66: 1182-1192
629

FIGURES

Figure 1 - Hepatic JNK-deficiency alters bile acid production and causes the development of cholestasis.

A L^{WT} and L^{DKO} mice at 6 months of age were fasted overnight and blood was collected. The amount of bile acids in the blood was measured (mean ± SEM; n = 6-11). Statistically significant differences between L^{DKO} and L^{WT} are indicated (**, $P < 0.01$).

B The composition of bile fluid collected from the gall bladder was examined by measurement of the ratio of bile acids (BA) to cholesterol (Chol) or phosphatidylcholine (PC) and the different type of BA. The data presented are the mean ± SEM (n = 4-5). Statistically significant differences between L^{DKO} and L^{WT} are indicated (*, $P < 0.05$; **, $P < 0.01$).

C L^{KO} and L^{WT} mice (age 6 months) were fasted overnight prior to removal of the liver. The expression of genes related to cholesterol synthesis (*Hmgcr* and *Hmgcs1*) and bile synthesis (*Cyp7a1*, *Cyp7b1*, *Cyp27a1, Baat*, *Cyp27a*, *Cyp8b1*) was measured by quantitative RT-PCR (mean ± SEM; n = 5-6). The expression was normalized to the amount of *18S* RNA in each sample. Statistically significant differences between LD^{KO} and L^{WT} are indicated (*, P < 0.05; **, P < 0.01).

D Representative liver sections stained with hematoxylin and eosin (H&E), an antibody to PCNA, and Masson Trichrome (Trichrome) are presented. Scale bar = 100 µm.

E The expression of genes related to inflammation was evaluated by RT-qPCR. (mean ± SEM; n = 5-6). The expression was normalized to the amount of *18S* RNA in each sample. Statistically significant differences between LD^{KO} and L^{WT} are indicated (*, P < 0.05).

F Liver damage was assessed from serum measurements of ALT, AST and γ-GT. (mean ± SEM; n = 11-24). Statistically significant differences between LD^{KO} and L^{WT} are indicated (*, P < 0.05; **, P < 0.01, ***, P < 0.001).

Figure 2 - Hepatic JNK-deficiency progress to cholangiocarcinoma through ERK activation.

A Representative livers of L^{WT} and L^{DKO} mice at age 14 months are shown.

B Representative sections of the liver of 14 month old chow-fed L^{DKO} mice were stained with hematoxylin and eosin (H&E) and Masson Trichrome (Trichrome). Scale bar = 100 µm.

C The liver mass and liver damage measured by levels of ALT and AST (mean ± SEM; n = 11-20) is presented. Statistically significant differences between LD^{KO} and L^{WT} are indicated (**, $P < 0.01$, ***, $P < 0.001$).

D Representative liver sections of 10 months old L^{DKO} and L^{WT} mice stained with glutamine synthetase (GS), Cytokeratin 19 (CK19) and Sox9. Scale bar = 50 µm.

E The expression of genes related to cholangiocytes proliferation was evaluated by RT-qPCR in 14-month-old L^{WT} and L^{DKO} mice (mean ± SEM; n = 5-6). Statistically significant differences between LD^{KO} and L^{WT} are indicated (*, $P < 0.05$; **, $P < 0.01$).

F The expression of genes related to the nuclear factor FXR (*Fxr*, *Fxrb*, *Shp, Fgr4*) and *Fgf15* was measured by quantitative RT-PCR in L^{WT} and L^{DKO} liver from mice at age 6 months (mean ± SEM; n = 5-6). Statistically significant differences between LD^{KO} and L^{WT} are indicated (*, $P < 0.05$; **, $P < 0.01$, ***, $P < 0.001$).

G Representative liver sections of 10-month-old L^{DKO} and L^{WT} mice stained with Phospho-ERK. Scale bar = 100 µm.

Figure 3 - PPARα deficiency reduces liver cancer induced by hepatic JNK-deficiency.

A Representative livers, tumor burden and incidence in 11 month old L^{WT}, L^{DKO} and $L^{PPAR\alpha DKO}$ mice (mean ± SEM; n = 14-25).

B The amount of bile acid in the blood was measured (mean ± SE; n = 7-11). The composition of bile fluid collected from the gall bladder was examined. Statistically significant differences between $L^{PPAR\alpha DKO}$, L^{DKO} and L^{WT} are indicated (*, P < 0.05; **, *P* < 0.01).

C The expression of genes related to cholesterol synthesis (*Hmgcr* and *Hmgcs1*), bile synthesis and transporters (*Cyp27a1, Baat*, *Cyp27a*, *Cyp8b1, Abcb11, Abcb4, Abcg5, Abcg8*), were measured by quantitative RT-PCR (mean ± SEM; n = 5-8). The amount of mRNA was normalized to the amount of *Gapdh* mRNA in each sample. Statistically significant differences between LD^{KO} and $L^{PPAR\alpha DKO}$ are indicated (*, P < 0.05; **, P < 0.01, ***, P < 0.001).

D Representative liver sections of 10-month-old L^{WT}, L^{DKO} and $L^{PPAR\alpha DKO}$ mice stained with glutamine synthetase (GS), Cytokeratin 19 (CK19) and Sox9. Scale bar = 100 μm.

E, F The expression of genes related to inflammation and cholangiocarcinoma was evaluated by quantitative RT-PCR. (mean ± SEM; n = 4-8). The expression was normalized to the amount of *Gapdh* mRNA in each sample. Statistically significant differences between LD^{KO} and $L^{PPAR\alpha DKO}$ are indicated (*, P < 0.05; **, P < 0.01, ***, P < 0.001).

G The expression of genes related to nuclear factor FXR pathway (*Fxr*, *Fxrb*, *Shp, Fgr4* and *Fgf15*) was evaluated in L^{KO} and $L^{PPAR\alpha DKO}$ livers by quantitative RT-PCR. (mean ± SEM; n = 6-8). The amount of mRNA was normalized to the amount of *Actin* mRNA in each sample. Statistically significant differences between LD^{KO} and $L^{PPAR\alpha DKO}$ are indicated (*, P < 0.05; **, P < 0.01).

H Representative sections of the liver of 10-month-old L^{DKO}, $L^{PPAR\alpha DKO}$ and L^{WT} mice stained with Phospho-ERK. Scale bar = 100 µm.

Figure 4 - Effect of PPARα deficiency on HCC in HFD-fed animals.

A Representative livers and H&E stained liver sections from diethylnitrosamine (DEN)-injected WT and PPARαKO mice fed a high fat diet (HFD) during 8 months. Scale bars = 1 cm / 0.5 mm.

B Quantification of tumor number and size in HFD-fed DEN-injected WT and PPARαKO mice. The maximum diameter of individual tumor nodules (central panel) and the mean width of tumor nodules (right panel) are presented. (mean ± SEM; n = 25). Statistically significant differences between WT and $L^{PPAR\alpha KO}$ are indicated (*, $P < 0.05$; **, $P < 0.01$, ***, $P < 0.001$).

C Kaplan-Meier analysis of HFD-fed DEN-injected WT and PPARαKO mice (Mantel-Cox log-rank test; n = 9-10).

D qRT-PCR analysis of cyclin and cell cycle regulator expression in liver samples from WT and PPARαKO mice. mRNA expression was normalized to *Gapdh* and WT liver expression (mean ± SEM, n = 5-6). Statistically significant differences between WT and PPARαKO mice are indicated (**, $P < 0.01$, ***, $P < 0.001$).

E-G WT and PPARαKO mice were fed HFD from 6 weeks of age. At 19 weeks, mice were injected i.p. with DEN (100 mg/kg) and sacrificed 48 h later.

E Immunoblot analysis of caspase3 and cleaved caspase3 in liver samples from untreated and acutely DEN-treated HFD-fed WT and PPARαKO mice. Vinculin protein expression was monitored as a loading control.

F Liver damage was assessed from serum measurements of ALT and AST; (mean ± SEM; n = 3-7). Statistically significant differences between WT and PPARαKO mice are indicated (**, P < 0.01, ***, P < 0.001).

G Immunoblot analysis of signaling pathways in liver samples from untreated and acutely DEN-treated WT and PPARαKO mice; blots were probed with antibodies to p-ERK, ERK, and p-STAT3. Vinculin expression was monitored as a loading control.

H WT and PPARαKO mice were injected i.p. on postnatal day 14 with DEN (50 mg/kg). At 8 weeks of age mice were lethally irradiated and inoculated i.v. with bone marrow cells from WT or PPARαKO mice. After 2 weeks, mice were place on the HFD and then sacrificed at 8.5 months of age. DEN-induced liver cancers in WT and PPARαKO mice transplanted with WT or PPARαKO bone marrow (BM genotype is indicated as super index of recipient mice). The bar chart shows mean tumor size, and photographs show representative images of livers from each condition. (mean ± SEM; n = 12-22); Statistically significant differences between WT and PPARαKO mice are indicated (**, P < 0.01, ***, P < 0.001).

TABLES

TABLE 1 - Taqman© assays probes – Related to RT-qPCR

Gene ID	Gene Name	Probe ID (Applied Biosystems)
Hmgcr	3-hydroxy-3-methylglutaryl-Coenzyme A reductase	Mm01282501_m1
Hmgcs1	3-hydroxy-3-methylglutaryl-Coenzyme A synthase	Mm00524111_m1
Cyp7a1	cytochrome P450, family 7, subfamily a, polypeptide 1	Mm00484152_m1
Cyp7b1	cytochrome P450, family 7, subfamily b, polypeptide 1	Mm00484157_m1
Baat	bile acid-Coenzyme A: amino acid N-acyltransferase	Mm00476075_m1
Cyp27a	cytochrome P450, family 27, subfamily a, polypeptide 1	Mm00470430_m1
Cyp8b1	cytochrome P450, family 8, subfamily b, polypeptide 1	Mm00501637_s1
Gpbar1	G protein-coupled bile acid receptor 1 (TGR5)	Mm00558112_s1
Shh	sonic hedgehog	Mm00436528_m1
Smo	smoothened homolog	Mm01162710_m1
Bmp4	bone morphogenetic protein 4	Mm00432087_m1
Scd1	stearoyl-Coenzyme A desaturase 1	Mm00772290_m1
Scd2	stearoyl-Coenzyme A desaturase 2	Mm01208542_m1
Chpt1	choline phosphotransferase 1	Mm00522694_m1
Chka	choline kinase alpha	Mm00442760_m1
Chkb	choline kinase beta	Mm00432498_m1
Cpt1	choline-phosphotransferase	Mm00550438_m1
Abcb11	ATP-binding cassette, sub-family B (MDR/TAP) , member 11	Mm00445168_m1
Atp8b1	ATPase, class I, type 8B, member 1	Mm01257688_m1
Slc10a1	solute carrier family 10 (sodium/bile acid cotransporter family) member 1	Mm00441421_m1

Slc10a2	solute carrier family 10, member 2	Mm00488258_m1
Abcb1a	ATP-binding cassette, sub-family B (MDR/TAP)	member 1A Mm00440761_m1
Abcb1b	ATP-binding cassette, sub-family B (MDR/TAP) member 1A	Mm01324120_m1
Abcc2	ATP-binding cassette, sub-family C (CFTR/MRP), member 2	Mm00496899_m1
Abcc3	ATP-binding cassette, sub-family C (CFTR/MRP), member 3	Mm00551550_m1
Abcc4	binding cassette, sub-family C (CFTR/MRP), member 4	Mm01226380_m1
Cd68	CD68	Mm00839636_g1
Ifng	Interferon gamma	Mm00801778_m1
Tnf	Tumor necrosis factor	Mm00443258_m1

748

749 ***TABLE 2 - qPCR primers - Related to RT-qPCR***

GENE	**Forward Primer**	**Reverse Primer**
Abcb11	TCTGACTCAGTGATTCTTCGCA	CCCATAAACATCAGCCAGTTGT
Abcb4	CAGCGAGAAACGGAACAGCA	TCAGAGTATCGGAACAGTGTCA
Abcg5	AGGGCCTCACATCAACAGAG	GCTGACGCTGTAGGACACAT
Abgc8	GTAGCTGATGCCGATGACAA	GGGGCTGATGCAGATTCA
Actb	GGCTGTATTCCCCTCCATCG	CCAGTTGGTAACAATGCCATGT
Baat	AGGTAAAGGAAAGCCGCATC	AGTCAATGACCCCTGGAAAA
Ccl2	TTAAAAACCTGGATCGGAACCAA	GCATTAGCTTCAGATTTACGGGT
Ccl3	TTCTCTGTACCATGACACTCTGC	CGTGGAATCTTCCGGCTGTAG
CcnA1	GCCTTCACCATTCATGTGGAT	TTGCTGCGGGTAAAGAGACAGAG
Cdc25c	ATGTCTACAGGACCTATCCCAC	ACCTAAAACTGGGTGCTGAAAC
Cdk2	CCTGCTCATTAATGCAGAGGG	GTGCTGGGTACACACTAGGTG

Cyp7a	GTCCGGATATTCAAGGATGCA	AGCAACTAAACAACCTGCCAGTACTA
Cyp7b1	AATTGGACAGCTTGGTCTGC	TTCTCGGATGATGCTGGAGT
Cyp8b1	CAGGAAGTTCCGTCGATTTG	GGCCCCAGTAGGGAGTAGAC
Cyp27a1	CCTCACCTATGGGATCTTCATC	TTTAAGGCATCCGTGTAGAGC
Elane	AGCAGTCCATTGTGTGAACGG	CACAGCCTCCTCGGATGAAG
f4/80	CCCCAGTGTCCTTACAGAGTG	GTGCCCAGAGTGGATGTCT
Fgfr4	TTGGCCCTGTTGAGCATCTTT	GCCCTCTTTGTACCAGTGACG
Foxm1	CTGATTCTCAAAAGACGGAGGC	TTGATAATCTTGATTCCGGCTGG
FxR	GCTTGATGTGCTACAAAAGCTG	CGTGGTGATGGTTGAATGTCC
FxRb	ACTCTCAGAGGTATCAGTCCTGC	CAGAGGTTGAGTCTTTCCCAC
Gapdh	TGAAGCAGGCATCTGAGGG	CGAAGGTGGAAGAGTGGGA
Hmgcr	AGCTTGCCCGAATTGTATGTG	TCTGTTGTGAACCATGTGACTTC
Hmgcs1	CAGGGTCTGATCCCCTTTG	GCAACGATTCCCACATCTTT
Il10	GCTCTTACTGACTGGCATGAG	CGCAGCTCTAGGAGCATGTG
Il1b	GCAACTGTTCCTGAATCAACT	ATCTTTTGGGGTCCGTCAACT
Il6	TAGTCCTTCCTACCCCAATTTCC	TTGGTCCTTAGCCACTCCTTC
Lyz2	ATGGAATGGCTGGCTACTATGG	ACCAGTATCGGCTATTGATCTGA
Nr5a2/LRH	TGAGGAACAACTCCGGGAAAA	CAGACACTTTATCGCCACACA
p19	CTGAACCGCTTTGGCAAGAC	GCCCTCTCTTATCGCCAGAT
p21	CCTGGTGATGTCCGACCTG	CCATGAGCGCATCGCAATC
p57	CGAGGAGCAGGACGAGAATC	GAAGAAGTCGTTCGCATTGGC
Shp	TGGGTCCCAAGGAGTATGC	GCTCCAAGACTTCACACAGTG
Gpbar1/TGR5	GCTAGGGCTCTCACCTGGA	CCCCAACACAGCAAGAAGAG
Tnf	CCCTCACACTCAGATCATCTTCT	GCTACGACGTGGGCTACAG

Trp53	CTCTCCCCCGCAAAAGAAAAA	CGGAACATCTCGAAGCGTTTA

EXPANDED VIEW FIGURES

Figure S1 - Effects of Hepatic JNK-deficiency liver.

L^{DKO} and L^{WT} mice (age 4 months) were fasted overnight prior to removal of the liver.

A, B The expression of genes related to phosphatidylcholine (PC) synthesis, hepatocyte-mediated transport of PC and BA was measured by quantitative RT-PCR. (mean ± SEM; n = 6-12). Gene expression was normalized to the amount of *18S* RNA in each sample. Statistically significant differences between L^{DKO} and L^{WT} are indicated (*, $P < 0.05$; **, $P < 0.01$).

C Representative liver sections stained with hematoxylin and eosin (H&E). Scale bar = 200 µm.

Figure EV2 - PPARα deficiency does not prevent HCC in mice fed a chow diet.

WT and PPARαKO mice (14 day old) were injected with DEN and maintained on a standard chow diet (normal diet; ND). Tumor number and size were quantified after sacrifice 13 months post DEN injection. (mean ± SEM; n = 8-14). ns = No statistically significant difference.

Figure EV3 - PPARα deficient mice on HFD exhibit defects in serum cytokines.

Luminex analysis of cytokines and chemokines in blood from WT and PPARαKO mice. Mice were fed a HFD during 13 weeks and left untreated or acutely treated with DEN for 48 h (100 mg/kg). Circulating cytokines were measured. Data are shown as means ± SEM

774 (n=4-7). Statistically significant differences between WT and PPARαKO mice are indicated
775 (*, P < 0.05; **, P < 0.01, ***, P < 0.001).
776
777 **Figure EV4 - Effect of PPARα-deficiency on liver cytokine expression.**
778 RT-qPCR analysis of liver and hepatic tumor cytokine and chemokine expression in WT
779 and PPARαKO mice. Mice were treated with DEN and maintained on the HFD for 8
780 months after DEN injection. The expression of genes coding for cytokines was measured
781 by quantitative RT-PCR. mRNA expression was normalized to *Gapdh* and to WT liver.
782 Data are shown as means ± SEM (n = 4-6). Statistically significant differences between
783 WT and PPARαKO mice are indicated (*, P < 0.05; **, P < 0.01).
784

A

B

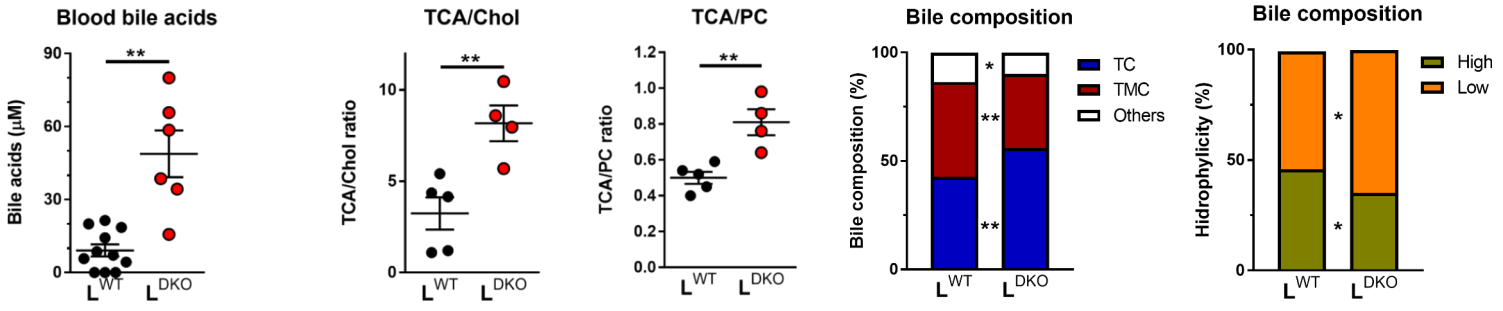

C

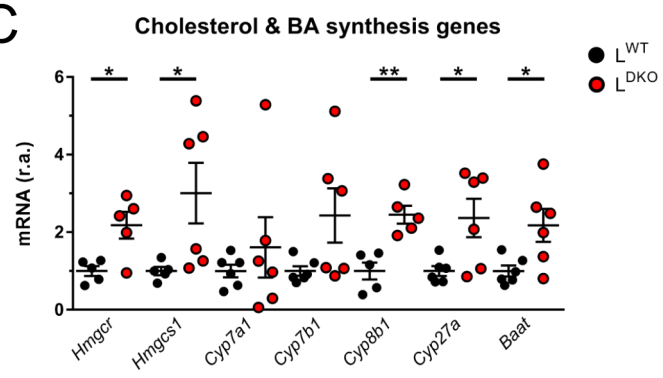

D

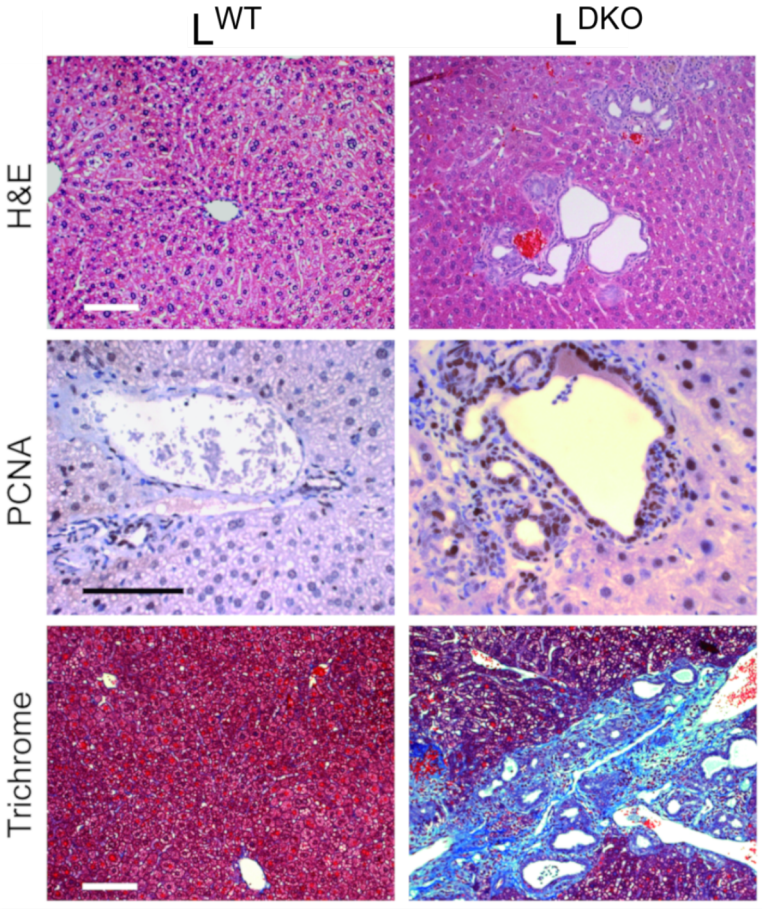

E

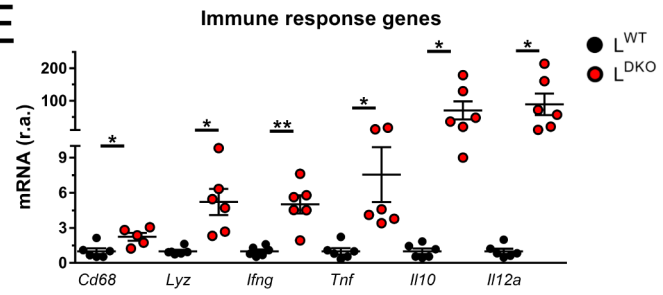

F

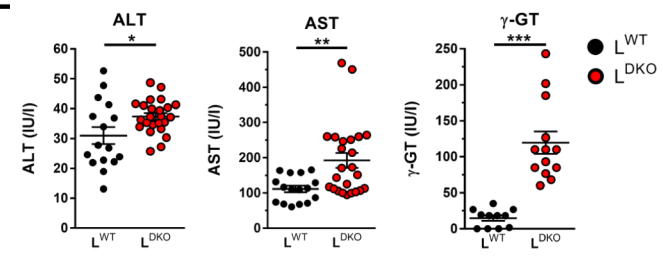

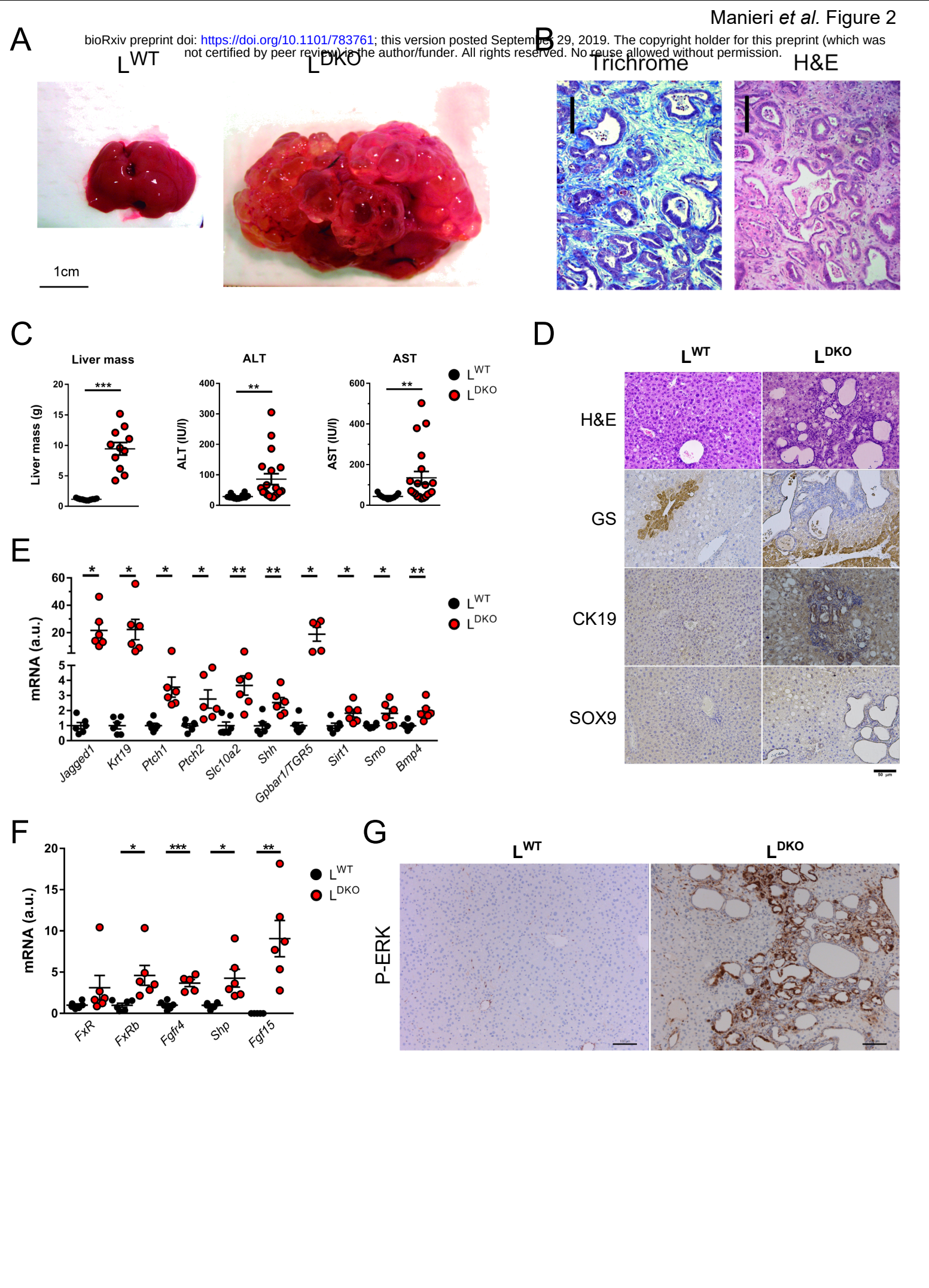

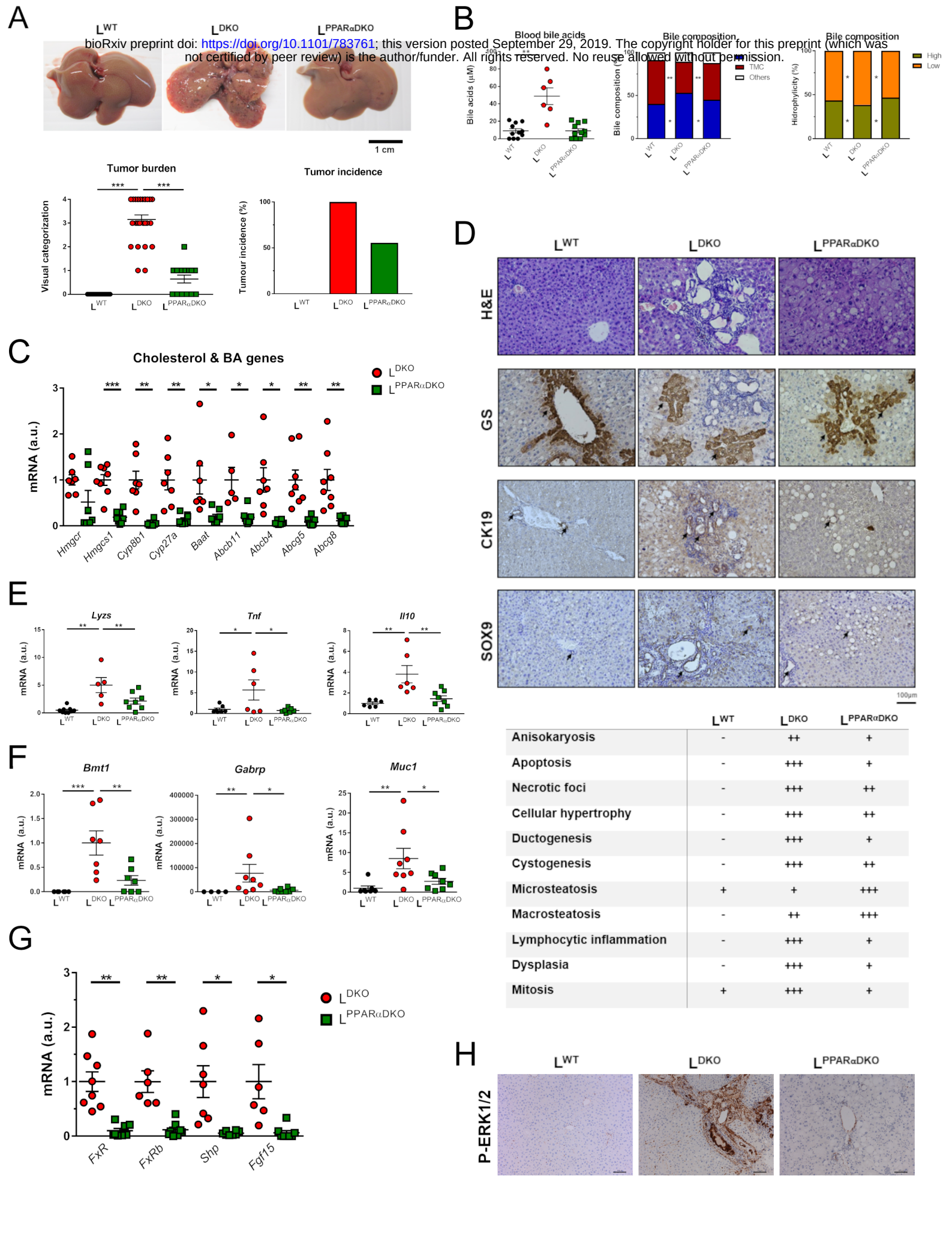

	L WT	L DKO	L PPARαDKO
Anisokaryosis	-	++	+
Apoptosis	-	+++	+
Necrotic foci	-	+++	++
Cellular hypertrophy	-	+++	++
Ductogenesis	-	+++	+
Cystogenesis	-	+++	++
Microsteatosis	+	+	+++
Macrosteatosis	-	++	+++
Lymphocytic inflammation	-	+++	+
Dysplasia	-	+++	+
Mitosis	+	+++	+

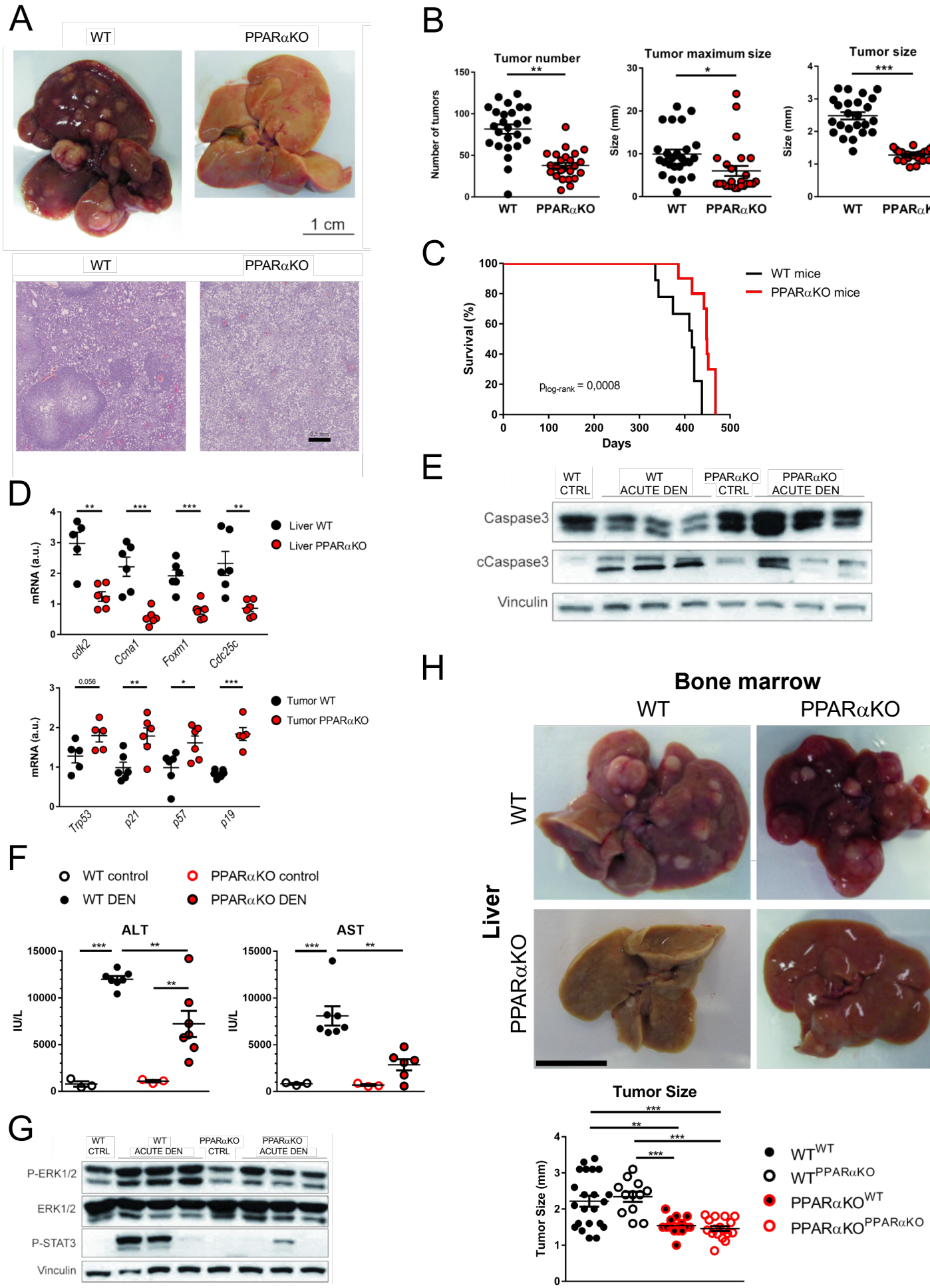
A
WT
PPARαKO
1 cm
WT
PPARαKO
B
Tumor number
Number of tumors
WT
PPARαKO
Tumor maximum size
Size (mm)
Tumor size
C
Survival (%)
Days
WT mice
PPARαKO mice
p log-rank = 0,0008
D
mRNA (a.u.)
Liver WT
Liver PPARαKO
cdk2
Ccna1
Foxm1
Cdc25c
Tumor WT
Tumor PPARαKO
Trp53
p21
p57
p19
E
WT CTRL
WT ACUTE DEN
PPARαKO CTRL
PPARαKO ACUTE DEN
Caspase3
cCaspase3
Vinculin
F
WT control
PPARαKO control
WT DEN
PPARαKO DEN
ALT
AST
IU/L
G
WT CTRL
WT ACUTE DEN
PPARαKO CTRL
PPARαKO ACUTE DEN
P-ERK1/2
ERK1/2
P-STAT3
Vinculin
H
Bone marrow
WT
PPARαKO
Liver
WT
PPARαKO
Tumor Size
Tumor Size (mm)
WT WT
WT PPARαKO
PPARαKO WT
PPARαKO PPARαKO

A

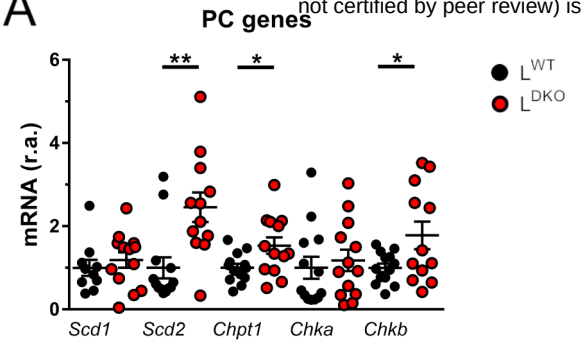

B

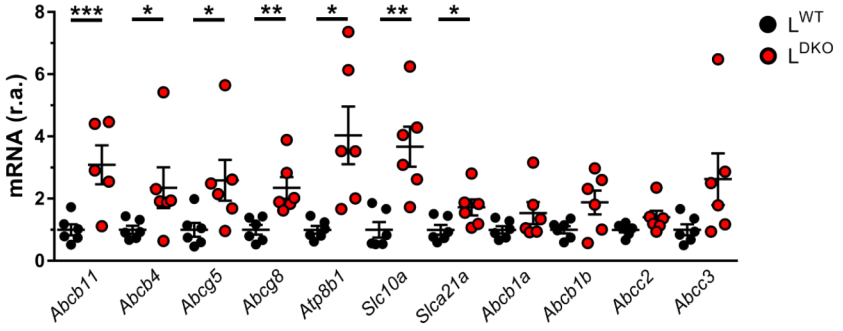

C

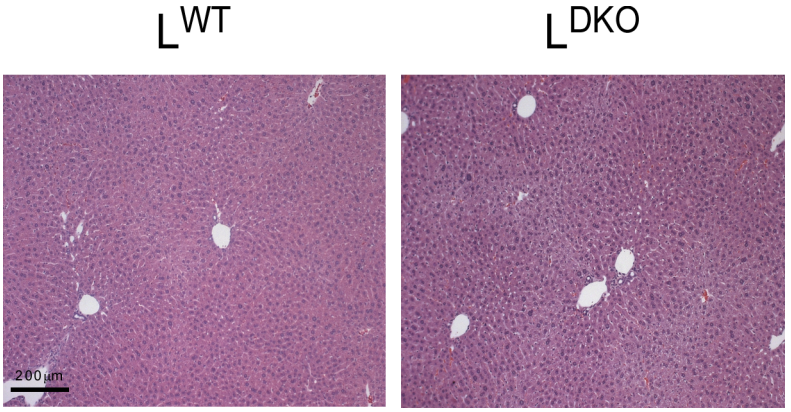

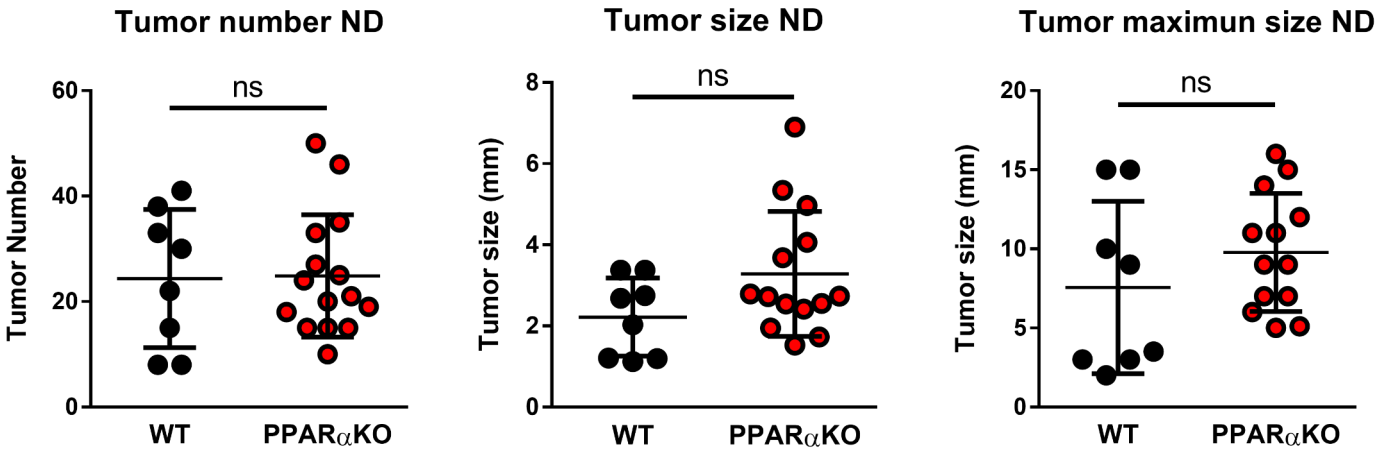

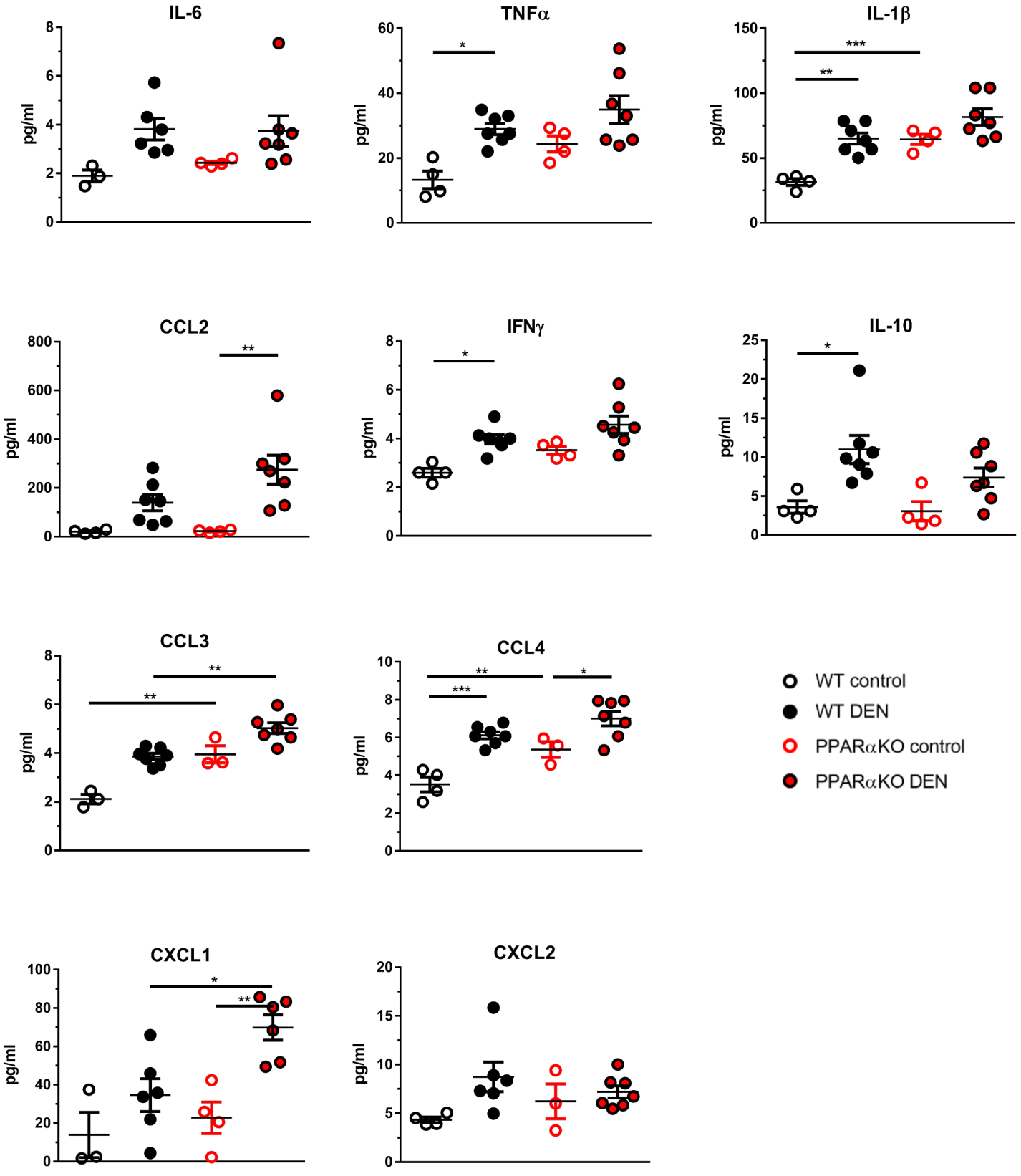

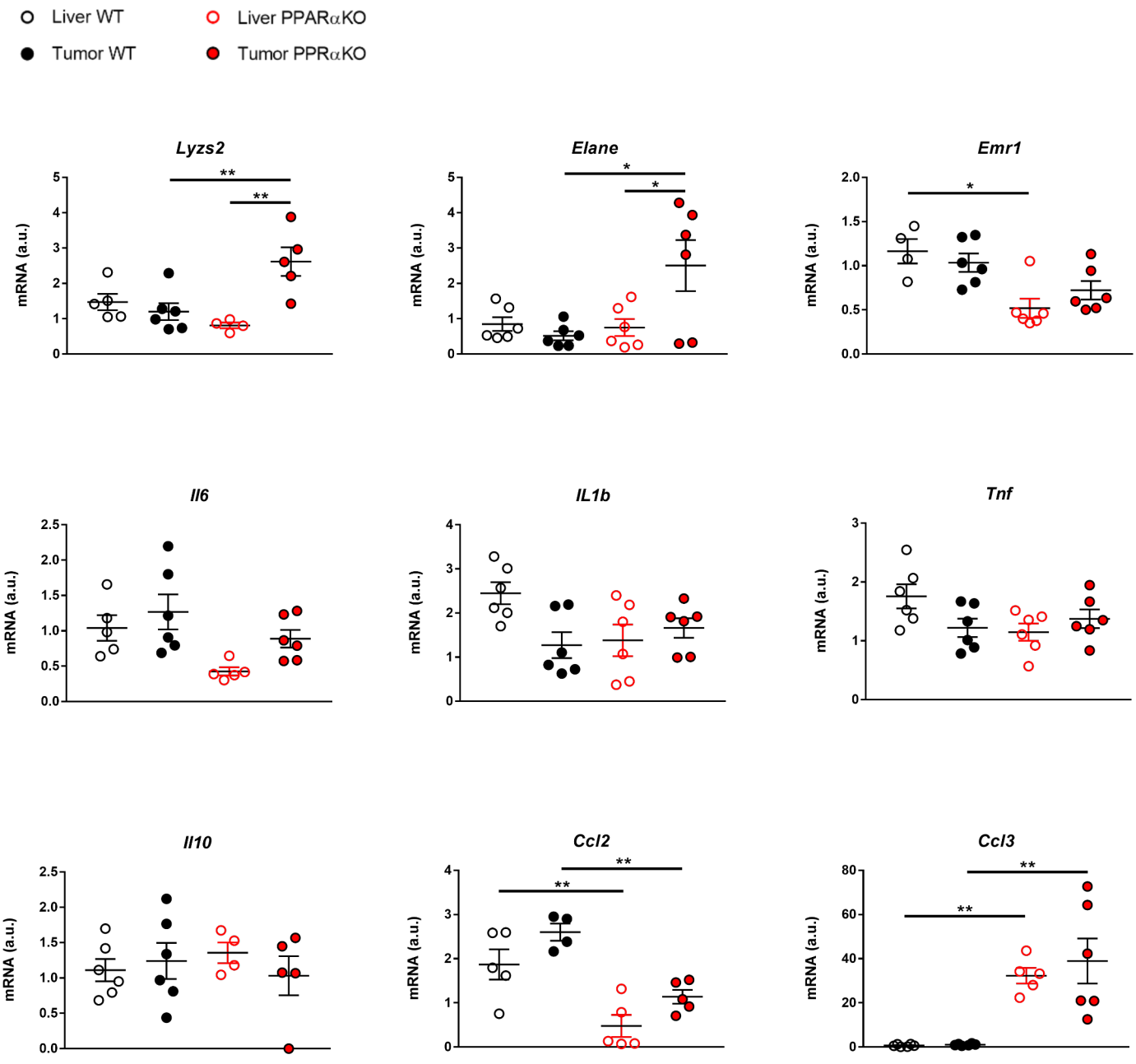
Liver WT
Liver PPARαKO
Tumor WT
Tumor PPRαKO
Lyzs2
Elane
Emr1
Il6
IL1b
Tnf
Il10
Ccl2
Ccl3
mRNA (a.u.)

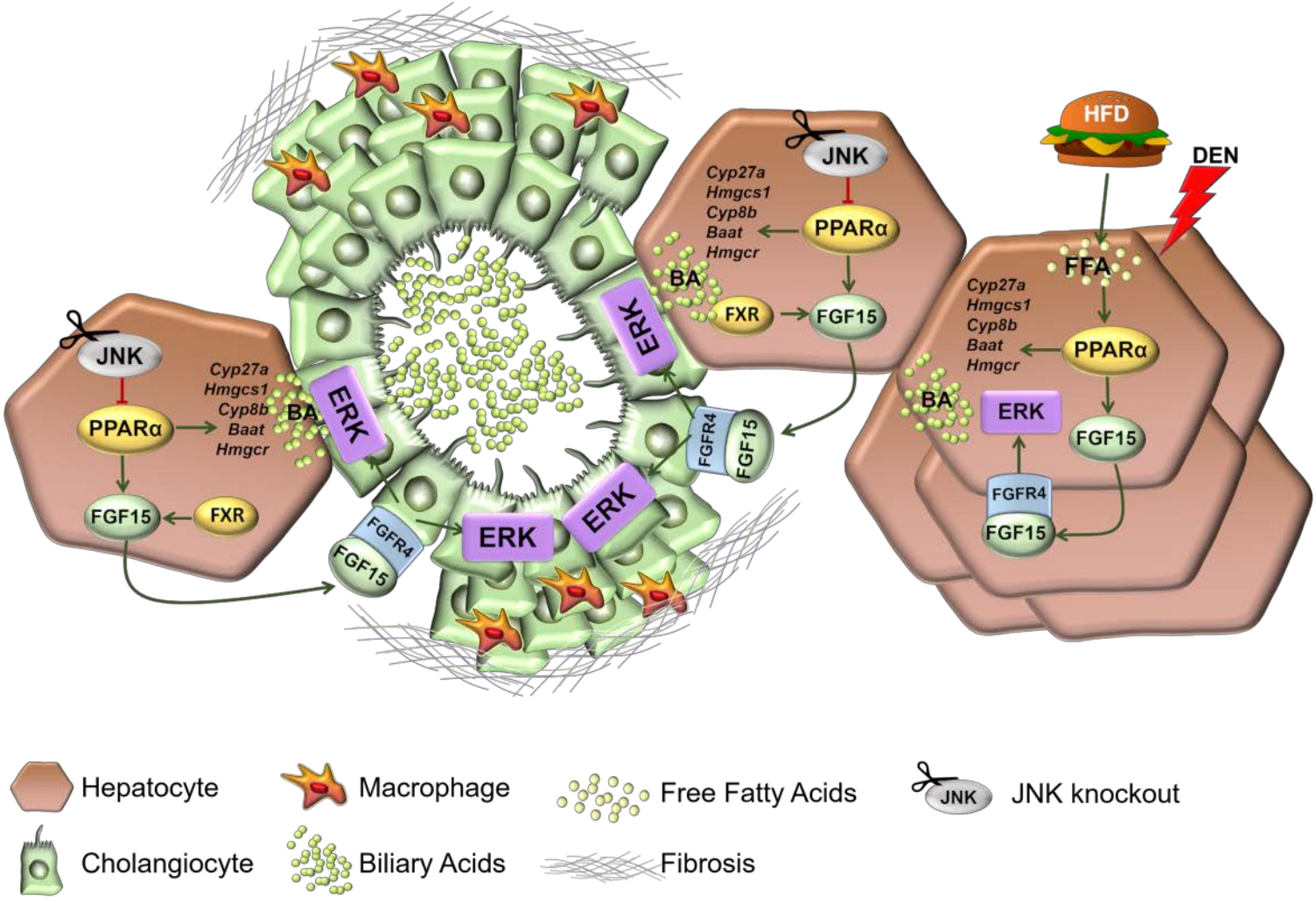
JNK
PPARα
Cyp27a
Hmgcs1
Cyp8b
Baat
Hmgcr
BA
FXR
FGF15
ERK
FGFR4
HFD
DEN
FFA
Hepatocyte
Macrophage
Free Fatty Acids
JNK knockout
Cholangiocyte
Biliary Acids
Fibrosis